

Robust seismic velocity change estimation using ambient noise recordings

E. Daskalakis¹, C. Evangelidis², J. Garnier³, N. Melis⁴, G. Papanicolaou⁵
and C. Tsogka⁶

¹ *Mathematics and Applied Mathematics, University of Crete and IACM/FORTH, GR-71409 Heraklion, Greece. (edaskala@iacm.forth.gr)*

² *Institute of Geodynamics, National Observatory of Athens, Athens, Greece. (cevan@noa.gr)*

³ *Laboratoire de Probabilités et Modèles Aléatoires & Laboratoire Jacques-Louis Lions, Université Paris VII, 75205 Paris Cedex 13, France. (garnier@math.univ-paris-diderot.fr)*

⁴ *Institute of Geodynamics, National Observatory of Athens, Athens, Greece. (nmelis@noa.gr)*

⁵ *Mathematics Department, Stanford University, Stanford, CA 94305. (papanicolaou@stanford.edu)*

⁶ *Mathematics and Applied Mathematics, University of Crete and IACM/FORTH, GR-71409 Heraklion, Greece. (tsogka@uoc.gr)*

SUMMARY

The estimation of seismic wave velocity changes from ambient noise recordings has been recently developed as part of passive seismology, a methodology that allows for extracting information about the structure of the earth using only passive noise recordings. The velocity change estimation is performed by comparing the cross-correlation function of two seismic station recordings as obtained at the current state with one that corresponds to a reference state. This is a challenging problem especially in the case of volcanic islands, or more generally, areas of interest that are not well equipped, and where only sparse seismic networks are available. Motivated by (Zhan et al., 2013) we want to study how seasonal fluctuations in the noise

sources may affect the velocity change estimation. We consider therefore a numerical model and introduce seasonal fluctuations in the amplitude spectra of the noise sources. We show that indeed, as pointed out in (Zhan et al., 2013), the stretching method is affected by these fluctuations and produces misleading apparent velocity variations which effectively reduce dramatically the signal to noise ratio of the method. We also show that this can be avoided by an adequate normalization of the cross-correlation functions. Theoretically we expect our approach to work as long as the seasonal fluctuations in the noise sources are uniform, an assumption which holds for closely located seismic stations. We illustrate with numerical simulations and real measurements that this modification significantly improves the accuracy of the velocity change estimation.

Key words: Time-series analysis, Interferometry, coda waves, crustal structure, seismic noise

1 INTRODUCTION

We are interested in monitoring volcanic edifices for temporal changes of the velocity of the seismic waves. When magma pressure increases inside a volcano, the added pressure results into the inflation of the volcano, and small cracks around the magma chamber will decrease the velocity of seismic waves. That small decrease in velocity can be detected using travel time tomography of seismic waves and up until very recently only the seismic waves generated by natural events like earthquakes could be used (Poupinet et al., 1984 ; Ratdomopurbo and Poupinet, 1995 ; Grêt et al., 2005). There are however limitations that make the use of such seismic events not suitable for monitoring, like the repeat rate or the unknown source position. In recent years ambient seismic noise recordings have been successfully used instead of seismic events (Breguier et al., 2008b ; Duputel et al., 2009).

The idea that has been exploited is that information about the Green's function or the travel time between two seismic stations can be obtained from cross-correlations (CC) of ambient noise recordings (Curtis et al., 2006 ; Schuster, 2009 ; Garnier and Papanicolaou, 2009 ; Wapenaar et al., 2010a ; Wapenaar et al., 2010b). A number of passive imaging studies based on this idea are now used in volcano monitoring (Breguier et al., 2008b), (Duputel

et al., 2009), in seismic faults studies (Breguier et al., 2008a ; D. et al., 2014) and more generally in studying the structure of the crust (D. et al., 2014 ; Sens-Schönfelder and Larose, 2010). In the case of volcano monitoring, there is a large number of studies concerning Piton de la Fournaise, which is a shield volcano on the eastern side of Reunion island in the Indian Ocean. The goal in this setting is to measure relative velocity changes (dv/v) of surface waves which are precursors to specific events (volcanic eruptions). Two techniques have been used for dv/v measurements, the moving window cross spectral (MWCS) method (Clarke et al., 2011) and the Stretching Method (SM).

Both MWCS and SM use two waveforms, the reference and the current CC functions which are obtained by averaging daily CC functions over a large, respectively a small, period of time. Changes in the velocity of the medium are estimated from differences in these two CC functions. In MWCS, dv/v is obtained by estimating the time delays dt_i in different time windows. The time delay estimation is performed in the frequency domain using the cross spectrum of the windowed wavefront segments. Then $dv/v(= -dt/t)$ is computed using a linear regression approach. SM operates in the time domain by solving an optimization problem which determines the stretching parameter that maximizes the correlation between the two waveforms.

There are some factors such as the quality and the distribution of the noise sources that can affect the temporal resolution of the measurements. The volcano of Piton de la Fournaise is a very well equipped area with lots of high quality stations. Moreover the type of the volcano (shield volcano), which is erupting very frequently, makes it an ideal example for study. That is not the case for most other volcanoes, especially for volcanic islands and "ring of fire volcanoes" which are poorly equipped and which erupt rarely. Another difficulty is that in some cases, and especially in the case we will consider in this paper, the evolution of the volcano is very slow and therefore long term fluctuations such as seasonal variations (Zhan et al., 2013 ; Meier et al., 2010) can hide velocity variations that actually correspond to volcanic activity.

In (Zhan et al., 2013) it is stated that the seasonal variations in the cross-correlations and the estimated velocity such as observed in (Meier et al., 2010) are caused by seasonal variations of the amplitude spectra of the ambient noise sources. Since SM operates directly in the time domain it is much more likely to be affected by those seasonal variations than the MWCS method which only relies on the phase spectra of the cross-correlations.

We present here a set of numerical simulations that leads to the conclusion that indeed the

stretching method can produce apparent velocity variations caused by seasonal fluctuations of the amplitude spectra of the noise sources. When these seasonal fluctuations are uniform with respect to the noise source locations, an hypothesis that is reasonable when the measurements concern recordings at the same area, the apparent velocity variations can be effectively removed by an adequate normalization (spectral whitening) of the cross-correlated signals.

2 SEASONAL VARIATIONS AND THE EFFECTIVENESS OF SPECTRAL WHITENING

By measuring velocity variations for a long enough period using the stretching method in (Meier et al., 2010), small seasonal variations were observed, which were attributed to hydrological and thermoelastic variations. In contrast, (Zhan et al., 2013) suggests that such apparent velocity variations could be caused by seasonal variations in the amplitude spectra of the noise sources and they are not necessarily due to changes in the medium. We will investigate here this question using numerically simulated data, as well as seismic noise recordings. Let us first briefly review the MWCS and the SM methods.

2.1 Description of the moving window cross-spectral method and the stretching method

Two methods have been predominately used for the estimation of velocity variations: the Stretching Method (SM) and the Moving Window Cross-Spectral (MWCS) method (Clarke et al., 2011).

In both methods, relative changes in the velocity of the medium are estimated by comparing two waveforms: the reference and the current cross-correlation functions which are obtained by cross-correlating the signals recorded at two different receivers over a certain period of time. The reference cross-correlation is usually the average of the daily cross-correlations over a long period of time of the order of a year. The current cross-correlation is a local average of the daily cross-correlation over a few days.

SM operates in the time domain and computes the stretching parameter that maximizes the correlation coefficient between the two waveforms in a selected time window. More precisely, if $CC_r(t)$ and $CC_c(t)$ denote the reference and the current cross-correlation functions, then SM seeks for the stretching coefficient $\epsilon = dt/t = -dv/v$ that maximizes the following

quantity,

$$C(\epsilon) = \frac{\int_{t_1}^{t_2} \text{CC}_{c,\epsilon}(t)\text{CC}_r(t)dt}{\sqrt{\int_{t_1}^{t_2} (\text{CC}_{c,\epsilon}(t))^2 dt} \sqrt{\int_{t_1}^{t_2} (\text{CC}_r(t))^2 dt}}, \quad (1)$$

where $\text{CC}_{c,\epsilon}(t) = \text{CC}_c(t(1 + \epsilon))$ is the stretched version of $\text{CC}_c(t)$. The time window $[t_1, t_2]$ is usually selected so as to contain the coda part of the cross-correlation function and not the first arrival.

The MWCS method is described in detail in (Clarke et al., 2011) and basically consists in computing time delays (dt_i) in different time windows and then estimating dt/t using a linear regression model. The relative velocity change in the medium is deduced by the relationship $dv/v = -dt/t$. The estimation of the time delays dt_i between the reference and the current cross-correlation is performed by computing phase differences in the frequency domain.

In (Meier et al., 2010) seasonal variations of the velocity within the Los Angeles basin were estimated using SM and it was suggested that possible reasons are hydrological or thermoelastic variations. In (Zhan et al., 2013) the authors suggest that the reason behind the seasonal variations is seasonal changes in the power spectral density of the noise sources. In this paper we use a simplified numerical model to study the effect of different types of seasonal changes of the noise sources in the velocity measurements.

2.2 The numerical model

We carry out a set of numerical simulations that are based on a mathematical model of wave propagation in homogeneous medium. The details of the numerical model are presented in the appendix; here we present some basic elements and the results of those simulations. In our numerical model we consider the acoustic wave equation:

$$\frac{1}{c(\mathbf{x})^2} \frac{\partial^2 u}{\partial t^2}(t, \mathbf{x}) - \Delta_{\mathbf{x}} u(t, \mathbf{x}) = n(t, \mathbf{x}), \quad (2)$$

where $n(t, \mathbf{x})$ models the noise sources which are located on a circle of radius 25km as illustrated in Figure 1. We assume that the wave field is recorded at two receivers $\mathbf{x}_1 = (-5, 0)$ km and $\mathbf{x}_2 = (5, 0)$ km.

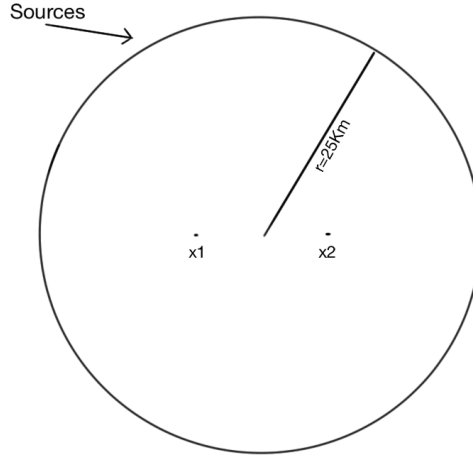


Figure 1. Location of the noise sources and the receivers at \mathbf{x}_1 and \mathbf{x}_2 .

The solution of (2) in a homogeneous medium at a given point \mathbf{x} can be written as,

$$u(t, \mathbf{x}) = \int \int G^j(t - s, \mathbf{x}, \mathbf{y}) n(s, \mathbf{y}) d\mathbf{y} ds, \quad (3)$$

or equivalently in the frequency domain,

$$\hat{u}(\omega, \mathbf{x}) = \int \hat{G}^j(\omega, \mathbf{x}, \mathbf{y}) \hat{n}(\omega, \mathbf{y}) d\mathbf{y}. \quad (4)$$

Here j denotes the dependence on the day, hat denotes the Fourier transform and $\hat{G}^j(\omega, \mathbf{x}, \mathbf{y})$ is the Green's function, which in a homogeneous medium is given by

$$\hat{G}^j(\omega, \mathbf{x}, \mathbf{y}) = \frac{1}{4\pi|\mathbf{x} - \mathbf{y}|} e^{i\frac{\omega}{c^j}|\mathbf{x} - \mathbf{y}|}. \quad (5)$$

In our model, the medium is homogeneous but its velocity is allowed to change as a function of time on the scale of a day. We denote by c^j the homogeneous velocity of the medium on day j .

REFERENCE AND CURRENT CROSS-CORRELATION FUNCTION

Our main tool, the daily cross-correlation function is given by

$$\text{CC}^j(\tau, \mathbf{x}_1, \mathbf{x}_2) = \frac{1}{T} \int_0^T u^j(t + \tau, \mathbf{x}_1) u^j(t, \mathbf{x}_2) dt, \quad (6)$$

with $T = 24$ hours.

In both SM and MWCS methods, variations in the velocity are estimated by comparing two waveforms: the reference and the current cross-correlation functions. The reference cross-

correlation will be the average of all the available daily cross-correlation functions,

$$\text{CC}_r(\tau, \mathbf{x}_1, \mathbf{x}_2) = \frac{1}{N_d} \sum_{j=1}^{N_d} \text{CC}^j(\tau, \mathbf{x}_1, \mathbf{x}_2), \quad (7)$$

where N_d is the total number of days, while the current cross-correlation function that corresponds to the j -th day will be the average of a small number of daily cross-correlation functions around the j -th day:

$$\text{CC}_c^j(\tau, \mathbf{x}_1, \mathbf{x}_2) = \frac{1}{2s+1} \sum_{k=j-s}^{j+s} \text{CC}^k(\tau, \mathbf{x}_1, \mathbf{x}_2). \quad (8)$$

The total number of daily cross-correlations used for the current cross-correlation is $N_{ccc} = 2s + 1$. Usually a few days ($N_{ccc} = 3$ to 10) are used for the current cross-correlation while the reference one is computed for a much longer period of the order of a year (Clarke et al., 2011).

Velocity Model and selected bandwidth

We will work in the frequency bandwidth [0.15 – 0.65]Hz and the total number of days is $N_d = 360$ (we call this a year). For our simulations we consider two different velocity models, in the first case the velocity of the medium does not change with time and is equal to 1Km/s while in the second case there is a small change in the velocity of the order of 1% that takes place between days 80 to 110. The velocity increases linearly the first 15 days until it reaches the maximal value of 1.01Km/s and then decreases linearly with the same rate to its original value of 1Km/s as illustrated in Figure 2 (bottom plot). All these numbers are realistic and very similar to the values that we have in our seismic noise recordings of the Santorini volcano considered in section §3. We have chosen the numerical set up to be similar to the experimental set up so that the numerical results are meaningful to demonstrate that the conclusions extracted from the experimental data are reliable.

2.2.1 Estimation of the relative change in the velocity

We have implemented both SM and MWCS methods using as reference cross-correlation the average of all daily cross-correlation (360 days) and as current cross-correlation a $N_{ccc} = 7$ -day average around the day we make the measurement.

The results obtained by both methods for the two velocity models are shown in Figure 2. We can see that the results are comparable and both methods can recover the relative velocity

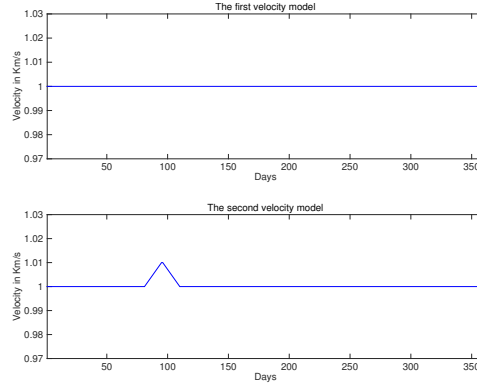


Figure 2. The two velocity models.

change up to a small error. We chose for the current cross-correlation a $N_{ccc} = 7$ -day average which minimizes the error in the estimation, as shown in Appendix A1.3 (see also Figure A2).

2.3 Seasonal variations in the noise sources and their influence to the relative velocity change measurements

Let us write equation (6) in the frequency domain using equations (A.1) and (4),

$$\widehat{CC}^j(\omega, \mathbf{x}_1, \mathbf{x}_2) = \int d\mathbf{y} \overline{\widehat{G}^j(\omega, \mathbf{x}_1, \mathbf{y})} \widehat{G}^j(\omega, \mathbf{x}_2, \mathbf{y}) \widehat{\Gamma}^j(\omega, \mathbf{y}). \quad (9)$$

Here $\omega \rightarrow \widehat{\Gamma}^j(\omega, \mathbf{y})$ is the power spectral density of the noise sources at location \mathbf{y} during day j (see Appendix A1.1). As a complex function, the cross-correlation can be written as a

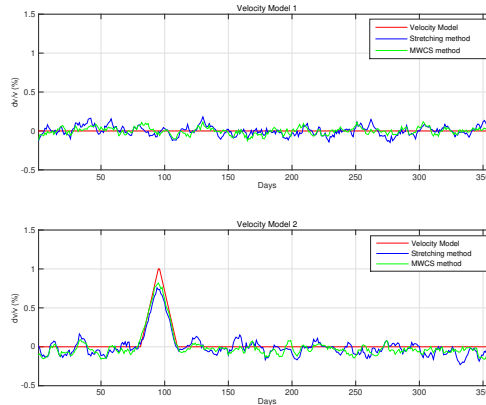


Figure 3. Relative velocity change estimation using SM (blue) and MWCS (green) for the constant (top) and the variable (bottom) velocity models of Figure 2.

product of an amplitude and a phase

$$\hat{\mathbb{C}}_j(\omega, \mathbf{x}_1, \mathbf{x}_2) = A_j(\omega, \mathbf{x}_1, \mathbf{x}_2)e^{i\phi_j(\omega, \mathbf{x}_1, \mathbf{x}_2)}. \quad (10)$$

We propose to use a normalization (spectral whitening) on the cross-correlation functions which consists in replacing the amplitude $A_j(\omega, \mathbf{x}_1, \mathbf{x}_2)$ by one in the frequency range where $A_j(\omega, \mathbf{x}_1, \mathbf{x}_2)$ is above a threshold. Therefore we get,

$$\hat{\mathbb{C}}_j(\omega, \mathbf{x}_1, \mathbf{x}_2) = e^{i\phi_j(\omega, \mathbf{x}_1, \mathbf{x}_2)}. \quad (11)$$

After this spectral whitening we expect that the seasonal variations that affect only the amplitude spectra of the cross-correlation function will not have an impact on the measurement of dv/v .

As shown in Appendix A1.4, when the seasonal variations of the noise sources are spatially uniform, then they affect only the amplitude spectra of the cross-correlations. Treating successfully the uniform case is important since we expect this hypothesis to be valid in most cases of interest where the receivers are close together geographically so that the seasonal variations are affecting in the same way, more or less, the ambient noise sources.

However, if the seasonal variations affect also the phase spectra of \mathbb{C} then the spectral whitening will not ensure that the measurement of dv/v will be free of apparent velocity changes due to seasonal variations of the noise sources. Our numerical model can simulate the daily perturbation of the power spectral density of the sources so as to be uniform or non-uniform with respect to the locations of the sources. The details of how this is implemented are in the appendix (see Appendix A1.4).

2.3.1 Results of numerical simulations

We use here our numerical model with the two different types of seasonal variations (uniform or non-uniform) and we study how these seasonal variations affect the estimations of the relative change in velocity when we use the stretching and the MWCS methods. We expect that in the case of the uniform daily perturbation, only the stretching method will be affected. Indeed, MWCS operates in the frequency domain and measures the phase difference between the two waveforms. Therefore, seasonal variations in the amplitude spectra of the cross-correlation as in (A.3) do not affect the estimation.

We also expect the seasonal variations in the amplitude spectra to be removed by the spectral whitening. This will eliminate the apparent seasonal variations and improve the estimations of the stretching method.

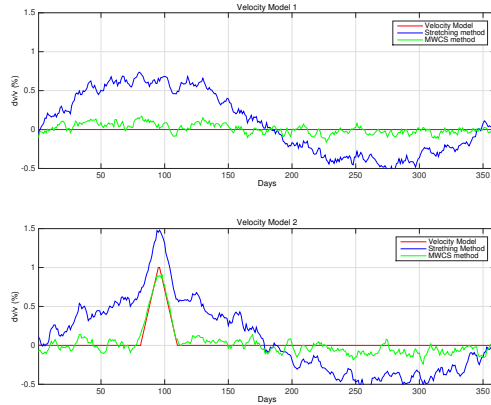


Figure 4. Relative velocity change for the first (top) and the second (bottom) velocity model using SM (blue) and MWCS (green) for the velocity models of Figure 2. Only the stretching method is affected by the seasonal variations since those are uniform with respect to the locations of the noise sources.

In the case of a non-uniform perturbation in the seasonal variations of the noise sources we expect that spectral whitening cannot eliminate their effect and we shall still observe apparent seasonal variations in the velocity. Note that in the latter case both methods (SM and MWCS) will lead to apparent velocity variations that are wrong and do not correspond to velocity changes in the medium.

We add first seasonal variations of a separable form using equation (A.4) and as we observe in Figure 4 only the stretching method reflects the seasonal variations of the noise sources into seasonal variations on the measurement of dv/v .

By using spectral whitening we correct for the seasonal variations in the amplitude of the cross-correlation function and as a result we expect to no longer observe seasonal variations in the measurements of dv/v when we use the stretching method. This is illustrated with our numerical results in Figure 5.

We do not expect to get the same result when the seasonal variations are of non-separable form as in equation (A.5). Indeed, we as we observe in Figure 6, spectral whitening cannot remove the seasonal variations any longer since those variations affect both the amplitude and phase spectra of the cross-correlation.

2.4 Seasonal variations examined in the island of Milos

Using the developed methodology we investigate here relative velocity changes in the quiet volcanic island of Milos. In the area two broadband seismic stations (codes: MHLO and

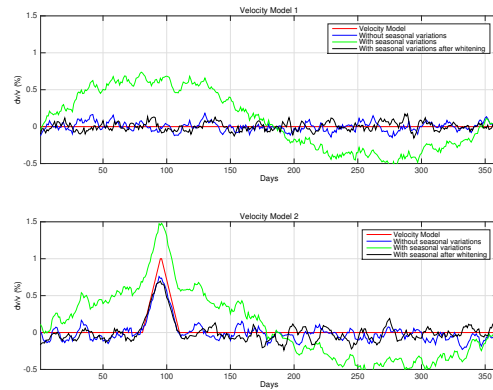


Figure 5. Comparison between the estimation obtained for the model without seasonal variations in blue (equation (A.2)), the model with uniform seasonal variations in green (equation (A.4)) and the effect of spectral whitening to the estimation in black for both velocity models. All estimations here are produced using the stretching method.

MHLA) operate in real time, monitoring seismicity in the Aegean volcanic arc for the National Observatory of Athens, Institute of Geodynamics (NOAIG) (Figure 7). The two stations are part of the Hellenic National Seismic Network (network code: HL) and they are deployed 6km apart and above the Milos island geothermal reservoir. We gather seismic noise recordings for the last days of 2011 and the entire 2012 and 2013 (827 days in total). During the examined period there was no significant local earthquake activity in the area. In Figure 8 we observe the seasonal variations on the Power Spectrum Density (PSD) of the station MHLA and we want to investigate if the stretching method is affected by those variations.

The data are filtered from 0.1–1.0Hz a bandwidth for which we have microseismic activity as suggested by figure 9. This frequency bandwidth will be used for Santorini in the next section since the power spectral density of the recorded signals is more or less the same.

As we see in Figure 10, the proposed normalization (spectral whitening) has the desirable

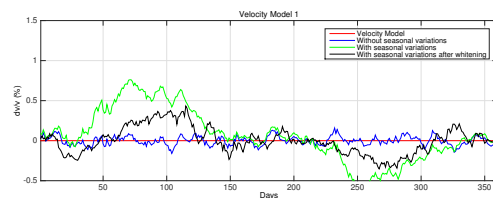


Figure 6. The estimation produced by the stretching method for the numerical model without seasonal variations in blue (equation (A.2)), the model of uniform seasonal variations in green (equation (A.5)) and the effect of spectral whitening to the estimation in black.

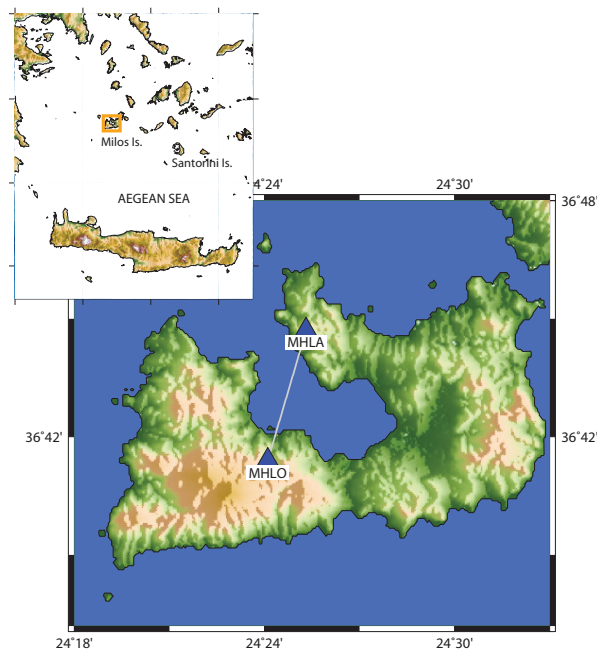


Figure 7. The volcanic island of Milos and the locations of the two NOAIG broadband seismic stations used in this study. The inset at the left hand side of the map shows the location of Milos island (orange rectangle) within the Aegean sea.

effect on seasonal variations just as the numerical simulations suggest. Considering the apparent velocity fluctuations induced by seasonal variations of the noise sources, as measurement noise, we obtain a decrease in the noise level of the order of 3 after using the proposed normalization. Using the stretching method with spectral whitening, we observe residual fluctuations in the estimated velocity of the order of $\pm 0.1\%$.

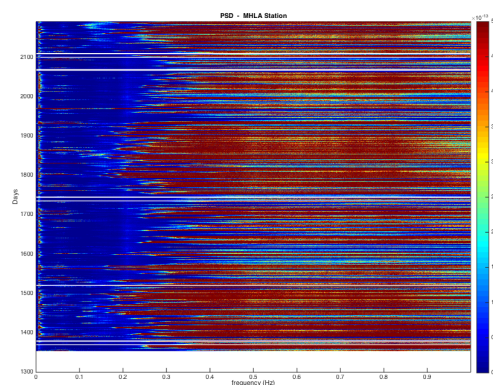


Figure 8. The Power Spectrum Density of the station MHLA at Milos.

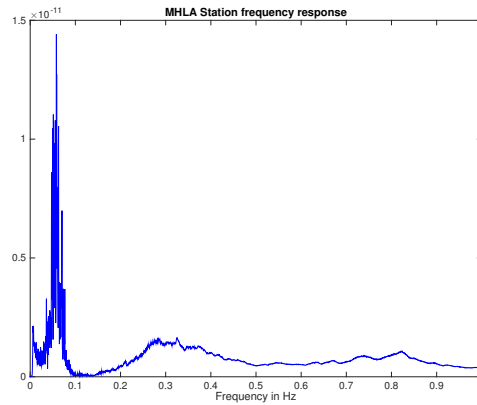


Figure 9. The frequency response of the MHLA station calculated by averaging the daily frequency response of all available days.

3 INVESTIGATION OF THE SANTORINI ISLAND SEISMIC UNREST 2011-2012

During the time period January 2011 to March 2012, high microseismic activity was observed in the caldera of the Santorini island (Figure 13). This also coincided with a 10cm uplift measured by GPS stations deployed in the area, monitoring continuously crustal deformation (Newman et al., 2012). During the unrest period, several portable seismic stations were deployed in the area by research institutions and universities. However, due to the urgency of the ongoing unrest, the portable stations were deployed mainly to monitor seismicity in near real time and thus, their data quality and/or availability was not suitable for ambient noise monitoring. Prior to the unrest, only two digital broadband seismic stations were in operation (Figure 11). These two were found useful to use for investigating variations in dv/v using the stretching method. Their inter-station path crosses the edge of the uplifted area within the caldera which is also the source region of the majority of the observed seismic clusters (Konstantinou et al., 2013).

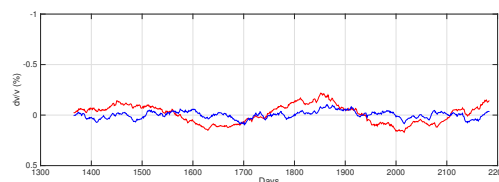


Figure 10. The estimation between the pair MHLO-MHLA located on the island of Milos when we use spectral whitening (blue) and when we do not use it(red). Here $N_{ccc} = 21$ Days.

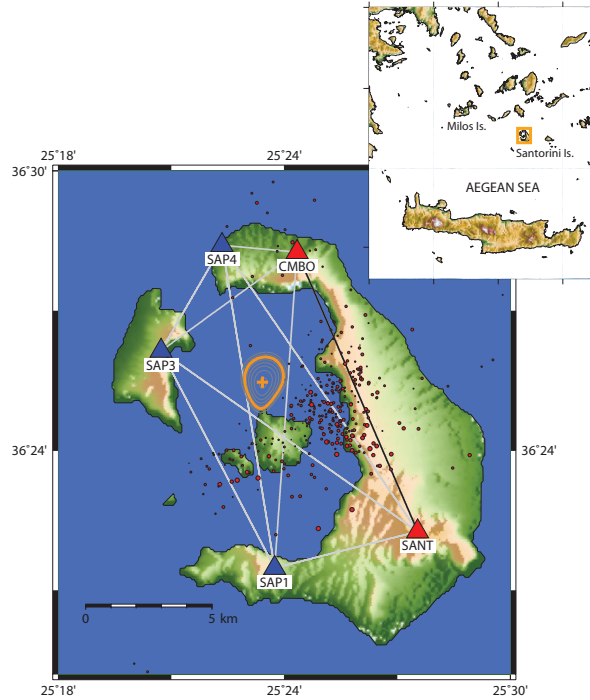


Figure 11. Network of seismic stations in Santorini and the inter-station paths. Stations that were in operation prior the unrest are marked in red. Stations that became operational during or after the unrest are marked in blue. Red circles indicate the relocated seismicity according to (Konstantinou et al., 2013) with their size being proportional to the event local magnitude (M_L) as measured by NOAIG. The orange cross marks the geographic location of the modeled volumetric growth at 4 km depth (Newman et al., 2012) with their 95% confidence level (concentric circle). The inset at the right hand side of the map shows the location of Santorini island (orange rectangle) within the Aegean sea.

The unrest was studied in (Lagios et al., 2013) and (Saltogianni et al., 2014) using GPS data and the results suggest elevation at the volcano mainly at periods with high seismicity. More specifically the seismic activity was high from January 2011 until August 2011 and then it is high again from October 2011 to February 2012. Those two periods of high seismicity are the same periods during which GPS data suggest that there is an elevation of the caldera.

3.1 Data Treatment

For each pair of stations we follow the next steps. First we separate the 24-hours long segment of each station into eight 3-hours segments. If a 3-hours long segment has more than 10% of gaps then it is rejected and will not be used in the calculations of the cross-correlation (CC). Otherwise, we filter the data in the band $[0.1 - 1.0]$ Hz. Then we apply one-bit normalization and we cross-correlate with the corresponding segment from the paired station. For each day

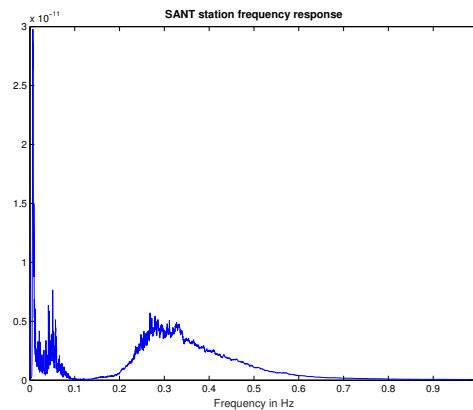


Figure 12. The frequency response of the SANT station calculated by averaging the daily frequency response of all available days.

we expect at most eight Cross-Correlation functions. If a 3-hour segment is rejected then we miss one cross-correlation and only if for one day we miss three or less cross-correlation functions we proceed and average the 3-hours segments to get the daily cross-correlation function. A final step that helps us to deal, under some conditions, with seasonal variations in the power spectral density of the noise sources, is to apply spectral whitening on the cross-correlations inside the bandwidth of interest, i.e., $[0.1 - 1.0]$ Hz.

For the reference cross-correlation function we use the mean of all available daily cross-correlation functions. The current cross-correlation function on the other hand is the mean of $N_{ccc} = 21$ days around the day where we want to make the measurement.

3.2 Results

Our implementation of the stretching method is configured to make two measurements of dv/v using the positive and the negative time axis in a time window that is focused on the coda part. ($[15, 35]$ s and $[-35, -15]$ in our case). The final result is the average of the two measurements as long as the correlation coefficient is higher than 0.7 otherwise the result is rejected.

Unfortunately we do not have data that cover the entire period of the unrest but as we can see in Figure (13) we can compare the available data with GPS data (from the GPS station NOMI).

The result shown in Figure 13 middle plot is quite close to the GPS measurements, at

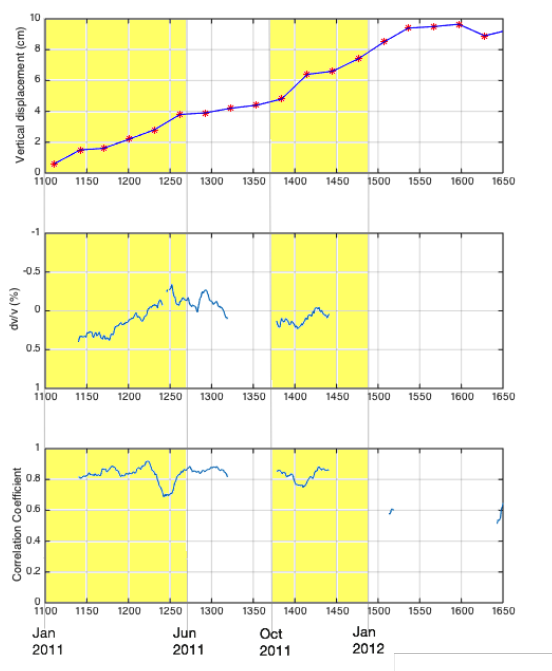


Figure 13. Top: Accumulated elevation of the GPS station NOMI in Santorini (Saltogianni et al., 2014). Middle: The estimation of dv/v using the stretching method. Bottom: The correlation coefficient of the stretching method.

least during the periods that we have available data and for the periods with high seismic activity (high seismic activity corresponds to the yellow background). We can also see that the elevation increases mainly at the periods of high seismic activity according to the GPS data (top plot at Figure 13).

Based on the data for Milos (Figure 10) and for Santorini in 2013 (Figure 14 ,red), the estimated velocity has random fluctuations of the order of $\pm 0.1\%$, resulting from residual seasonal variations and errors in the estimation. Therefore, any change of more than $\pm 0.1\%$ can be considered as significant, *i.e.*, resulting from physical changes in the velocity distribution. This is what happens in Santorini in 2011 (Figure 14, blue).

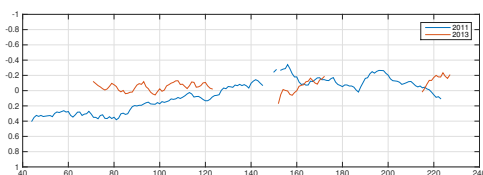


Figure 14. Results using Stretching method in two different years.

4 CONCLUSIONS

In this paper we considered the problem of seismic velocity change estimation based on passive noise recordings. Using simple but realistic numerical simulations as a tool, we study how the estimation produced by the stretching method is affected by seasonal fluctuations of the amplitude spectra of the noise sources (Zhan et al., 2013 ; Meier et al., 2010). Moreover, we show that an adequate normalization (spectral whitening) of the cross-correlation functions reduces the effect of the seasonal fluctuations of the noise sources. We also study the Santorini unrest event of 2011-2012, a slow event that spans over a period of several months, and for which it would be extremely difficult to follow the variations of dv/v without removing the seasonal fluctuations. Our results show a decrease in the velocity of seismic waves in the caldera of Santorini which is correlated with the accumulated elevation measured with GPS. This example illustrates the potential of developing monitoring tools which provide accurate results even with sparse seismic networks with careful signal processing of passive noise recordings.

ACKNOWLEDGEMENTS

The work of G. Papanicolaou was partially supported by AFOSR grant FA9550-11-1-0266. The work of J. Garnier was partially supported by ERC Advanced Grant Project MULTIMOD-26718. The work of E. Daskalakis and C. Tsogka was partially supported by the ERC Starting Grant Project ADAPTIVES-239959.

REFERENCES

- Brenguier, F., Campillo, M., Hadziioannou, C., Shapiro, N. M., Nadeau, R. M., and Larose, E. (2008a). Postseismic relaxation along the San Andreas fault at Parkfield from continuous seismological observations. *Science*, 321(5895):1478–1481.
- Brenguier, F., Shapiro, N. M., Campillo, M., Ferrazzini, V., Duputel, Z., Coutant, O., and Necessia, A. (2008b). Towards forecasting volcanic eruptions using seismic noise. *Nature Geoscience*, 1(2):126–130.
- Clarke, D., Zaccarelli, L., Shapiro, N., and Brenguier, F. (2011). Assessment of resolution and accuracy of the moving window cross spectral technique for monitoring crustal temporal variations using ambient seismic noise. *Geophys. J. Int.*, 186:867–882.
- Curtis, A., Gerstoft, P., Sato, H., Snieder, R., and Wapenaar, K. (2006). Seismic interferometry - turning noise into signal. *The Leading Edge*, 25:1082–1092.

- D., A., Bulut, F., Bohnhoff, M., and Kartal, R. (2014). Coseismic velocity change associated with the 2011 van earthquake (m7.1): Crustal response to a major event. *Geophys. Res. Lett.*, 41:4519–4526.
- Duputel, Z., Ferrazzini, V., Brenguier, F., Shapiro, N., Campillo, M., and Necessian, A. (2009). Real time monitoring of relative velocity changes using ambient seismic noise at the Piton de la Fournaise volcano (La Réunion) from January 2006 to June 2007. *J. of Volcanology and Geothermal Res.*, 184:164–173.
- Garnier, J. and Papanicolaou, G. (2009). Passive sensor imaging using cross correlations of noisy signals in a scattering medium. *SIAM J. Imaging Sciences*, 2:396–437.
- Grêt, A., Snieder, R., Aster, R. C., and Kyle, P. R. (2005). Monitoring rapid temporal change in a volcano with coda wave interferometry. *Geophys. Res. Lett.*, 32(L06304).
- Konstantinou, K., Evangelidis, C., Liang, W.-T., Melis, N., and Kalogeras, I. (2013). Seismicity, vp/vs and shear wave anisotropy variations during the 2011 unrest at Santorini caldera, southern Aegean. *Journal of Volcanology and Geothermal Research*, 267(0):57 – 67.
- Lagios, E., Sakkas, V., Novali, F., Bellotti, F., Ferretti, A., Vlachou, K., and Dietrich, V. (2013). SqueesarTM and {GPS} ground deformation monitoring of Santorini volcano (1992–2012): Tectonic implications. *Tectonophysics*, 594(0):38 – 59.
- Meier, U., Shapiro, N. M., and Brenguier, F. (2010). Detecting seasonal variations in seismic velocities within los angeles basin from correlations of ambient seismic noise. *Geophysical Journal International*, 181(2):985–996.
- Newman, A. V., Stiros, S., Feng, L., Psimoulis, P., Moschas, F., Saltogianni, V., Jiang, Y., Papazachos, C., Panagiotopoulos, D., Karagianni, E., and Vamvakaris, D. (2012). Recent geodetic unrest at Santorini caldera, Greece. *Geophysical Research Letters*, 39(6):n/a–n/a.
- Poupinet, G., Ellsworth, W., and Frechet, J. (1984). Monitoring velocity variations in the crust using earthquake doublets: An application to the calaveras fault, california. *J. Geophys. Res.*, 89(B7):5719–5731.
- Ratdomopurbo, A. and Poupinet, G. (1995). Monitoring a temporal change of seismic velocity in a volcano: application to the 1992 eruption of mt. merapi (indonesia). *Geophys Res Lett.*, 22(7):775–778.
- Saltogianni, V., Stiros, S. C., Newman, A. V., Flanagan, K., and Moschas, F. (2014). Time-space modeling of the dynamics of Santorini volcano (Greece) during the 2011–2012 unrest. *J. Geophys. Res. Solid Earth*, 119:8517–8537.
- Schuster, G. T. (2009). *Seismic interferometry*. Cambridge University Press, Cambridge.
- Sens-Schönfelder, C. and Larose, E. (2010). Lunar noise correlation, imaging and monitoring. *Earthquake Science*, 23(5):519–530.
- Wapenaar, K., Draganov, D., Snieder, R., Campman, X., and Verdel, A. (2010a). Tutorial on seismic interferometry: Part 1 - basic principles and applications. *Geophysics*, 75:A195–A227.
- Wapenaar, K., Slob, E., Snieder, R., and Curtis, A. (2010b). Tutorial on seismic interferometry: Part

2 - underlying theory and new advances. *Geophysics*, 75:A211–A227.

Zhan, Z., Tsai, V., and Clayton, R. (2013). Spurious velocity changes caused by temporal variations in ambient noise frequency content. *Geophys. J. Int.*, 194:1574–1581.

APPENDIX A: APPENDIX**A1 Description of the numerical model.**

In this section we give further details on the numerical model used in section 2.2.

A1.1 The noise sources.

The function $n(t, \mathbf{x})$ in equation (2) models the noise sources. We assume that it is a zero-mean random process. We also assume that the process is stationary in time with a covariance function that is delta correlated in space. Therefore, the covariance function of the noise sources has the form

$$\langle n(t_1, \mathbf{y}_1), n(t_2, \mathbf{y}_2) \rangle = \Gamma(t_2 - t_1, \mathbf{y}_1) \delta(\mathbf{y}_2 - \mathbf{y}_1). \quad (\text{A.1})$$

Here $\langle \cdot \rangle$ stands for statistical averaging. The function $t \rightarrow \Gamma(t, \mathbf{y})$ is the time correlation function of the noise signals emitted by the noise sources at location \mathbf{y} . The Fourier transform $\omega \rightarrow \hat{\Gamma}(\omega, \mathbf{y})$ is their power spectral density (by Wiener-Khintchine theorem). The function $\mathbf{y} \rightarrow \Gamma(0, \mathbf{y})$ characterizes the spatial support of the sources. In our case we assume that the sources are uniformly distributed on a circle \mathcal{C} of radius of $R_{\mathcal{C}} = 25\text{km}$ as illustrated in Figure 1:

$$\Gamma(t, \mathbf{y}) = \frac{1}{2\pi R_{\mathcal{C}}} \Gamma_0(t, \mathbf{y}) \delta_{\mathcal{C}}(\mathbf{y}).$$

We also assume that we have two receivers at $\mathbf{x}_1 = (-5, 0)\text{km}$ and $\mathbf{x}_2 = (5, 0)\text{km}$.

A1.2 Obtaining the time-series data at \mathbf{x}_1 and \mathbf{x}_2 .

To obtain data at \mathbf{x}_1 and \mathbf{x}_2 we define the exact distribution and power spectral density of the sources. From now on we assume that the statistics of the noise sources change from one day to another one and we denote by $\Gamma_0^j(t, \mathbf{y})$ its covariance function at day j . We take $N_s = 180$ point sources uniformly distributed on the circle of Figure 1 and then the equation (4) becomes

$$\hat{u}^j(\omega, \mathbf{x}) = \frac{1}{N_s} \sum_{i=1}^{N_s} \hat{G}^j(\omega, \mathbf{x}, \mathbf{y}_i) \hat{n}_i^j(\omega), \quad (\text{A.2})$$

where $\hat{n}_i^j(\omega)$ is the frequency content of the noise sources at \mathbf{y}_i during day j , which is random such that $\langle \hat{n}_i^j(\omega) \rangle = 0$ and

$$\langle \hat{n}_i^j(\omega) \overline{\hat{n}_i^j(\omega')} \rangle = 2\pi \hat{\Gamma}_0^j(\omega, \mathbf{y}_i) \delta(\omega - \omega').$$

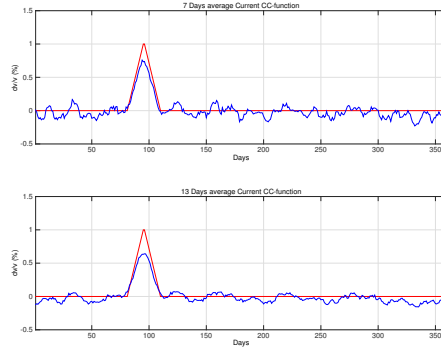


Figure A1. In the top plot $N_{ccc} = 7$ days are used in computation of the reference CC while $N_{ccc} = 13$ days are used in the bottom plot. In red is the true velocity variation and in blue the estimated one. Using $N_{ccc} = 7$ days gives a more precise estimation for the maximal value of dv/v while with $N_{ccc} = 13$ days the fluctuations around zero are decreased.

At first we consider that the noise sources do not have any seasonal variations and therefore their power spectral density does not depend on j . Later on that will be changed according to the model of seasonal variations we want to study. In either case, the last step in order to obtain the time series recorded at location \mathbf{x} is to apply the inverse Fourier transform to (A.2).

A1.3 Relation between the number of days used in the current CCfunction and the quality of the measurement obtained by the stretching method

There is a direct relation between the number of days N_{ccc} that are used in the current CCfunction and the standard deviation of the measurement error. When there is no velocity variations ($dv/v = 0\%$), the obvious answer is that the standard deviation of the error is reduced by increasing the number of days used in the computation of the current CC. However, this results to a loss in precision in the estimation of $dv/v \neq 0$ as illustrated by the results in Figure A1. An optimal value for the number of days to be used can be obtained by studying how the error changes as we increase the number of days N_{ccc} . The value we selected is 7 since for this value we have a minimum in the error as suggested by Figures A2 and A3, is $N_{ccc} = 7$ days.

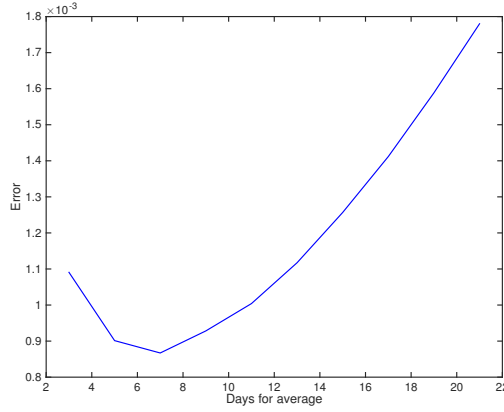


Figure A2. The relation between the number of days N_{ccc} stacked for the Current CCfunction and the error at the days 80 to 110 using the norm $\|x\| = \sqrt{\sum_{i=1}^m |x_i|^2}$, where $x \in \mathbf{R}^m$.

A1.4 Uniform and non-uniform seasonal variations.

Our model for the power spectral density of the noise sources is

$$\hat{\Gamma}_0^j(\omega, \mathbf{y}) = \hat{F}(\omega) \hat{s}^j(\omega, \mathbf{y}),$$

Here the unperturbed noise source distribution is uniform over the circle \mathcal{C} and has power spectral density $\hat{F}(\omega)$, and $\hat{s}^j(\omega, \mathbf{y})$ is the daily perturbation of the power spectral density at location \mathbf{y} . We have two different representations for \hat{s}^j :

- (i) The daily perturbation is uniform with respect to the locations of the sources: $\hat{s}^j(\omega, \mathbf{y}) = \hat{f}^j(\omega)l(\mathbf{y})$,

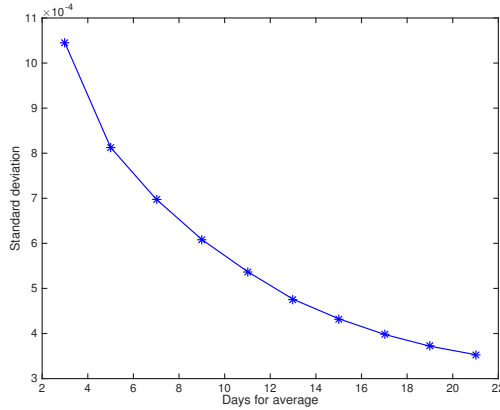


Figure A3. The relation between the number of days N_{ccc} stacked for the Current CCfunction and the standard deviation of the error in the period where $dv/v = 0$ (days 1 to 80 and 110 to 360).

(ii) The daily perturbation is not uniform and we cannot write it in a separable form.

In the first case equation (9) becomes

$$\begin{aligned} \hat{\mathbb{C}}^j(\omega, \mathbf{x}_1, \mathbf{x}_2) &= \hat{F}(\omega) \hat{f}^j(\omega) \\ &\times \int_{\mathcal{C}} d\sigma(\mathbf{y}) \overline{\hat{G}^j(\omega, \mathbf{x}_1, \mathbf{y})} \hat{G}^j(\omega, \mathbf{x}_2, \mathbf{y}) l(\mathbf{y}), \end{aligned} \quad (\text{A.3})$$

and it is clear that after spectral whitening, any daily perturbation in the power spectral density of the noise sources will be eliminated since the perturbation is contained into the amplitude spectra of the cross-correlation function. In the second case we cannot separate the terms due to the sources and take them out of the integral.

Instead of equation (A.2), we use,

$$\begin{aligned} \hat{u}^j(\omega, \mathbf{x}) &= \frac{1}{N_s} \sum_{i=1}^{N_s} \hat{n}_i^j(\omega) \hat{G}^j(\omega, \mathbf{x}, \mathbf{y}_i) \\ &\times (1 - \delta \hat{g}(\omega) \sin(2\pi j/N_d)), \end{aligned} \quad (\text{A.4})$$

with $\delta = 0.4$ and

$$\hat{g}(\omega) = \begin{cases} 1 & \text{if } \omega_1 \leq \omega \leq \omega_1 + \pi B, \\ 0 & \text{if } \omega_1 + \pi B < \omega \leq \omega_1 + 2\pi B, \end{cases}$$

to simulate uniform seasonal variations with

$$\hat{s}^j(\omega, \mathbf{y}) = (1 - \delta \hat{g}(\omega) \sin(2\pi j/N_d))^2.$$

In the simulations we take $\hat{F}(\omega) = \mathbf{1}_{[\omega_1, \omega_1 + 2\pi B]}(|\omega|)$, $B = 0.5\text{Hz}$ and $\omega_1 = 2\pi \cdot 0.15\text{rad}\cdot\text{s}^{-1}$.

For the non-uniform case, we use,

$$\begin{aligned} \hat{u}^j(\omega, \mathbf{x}) &= \frac{1}{N_s} \sum_{i=1}^{N_s} \hat{n}_i^j(\omega) \hat{G}^j(\omega, \mathbf{x}, \mathbf{y}_i) \\ &\times (1 - \delta \hat{g}(\omega; 2\pi i/N_s + 2\pi j/N_d) \sin(2\pi j/N_d)), \end{aligned} \quad (\text{A.5})$$

where

$$\hat{g}(\omega; \theta) = \begin{cases} 1 & \text{if } \omega_1 \leq \omega \leq \omega(\theta), \\ 0 & \text{if } \omega(\theta) < \omega \leq \omega_1 + 2\pi B, \end{cases}$$

with

$$\omega(\theta) = \omega_1 + \pi B + \pi B \sin(\theta). \quad (\text{A.6})$$

This models non-uniform seasonal variations with

$$\hat{s}^j(\omega, \mathbf{y}) = (1 - \delta \hat{g}(\omega; \theta(\mathbf{y}) + 2\pi j/N_d) \sin(2\pi j/N_d))^2,$$

where $\theta(\mathbf{y})$ is the angle of \mathbf{y} on the circle \mathcal{C} .